Journal of Computational Physics **178,** 533–562 (2002)
doi:10.1006/jcph.2002.7040, available online at http://www.idealibrary.com on IDEAL®

# A Well-Balanced Gas-Kinetic Scheme for the Shallow-Water Equations with Source Terms

Kun Xu[1]

*Department of Mathematics, Hong Kong University of Science and Technology, Clear Water Bay, Kowloon, Hong Kong*
E-mail: makxu@uxmail.ust.hk

Received June 5, 2001; revised December 7, 2001

This paper is about the extension of the gas-kinetic BGK scheme to the shallow-water equations with source terms. In the current study, the particle velocity change due to the gravitational force and variable river bottom is implemented explicitly in the flux evaluation. The current scheme is a well-balanced method, which presents accurate and robust results in both steady and unsteady flow simulations.


*Key Words:* shallow water equations; source terms; gas-kinetic scheme; gravitational force.

## 1. INTRODUCTION

In recent years, the study of a hyperbolic system with source terms has attracted much attention in the CFD community. One of the main reasons is that there exist wide engineering applications. For example, the Saint-Venant equations are widely used in ocean and hydraulic engineering to describe bore wave propagation, hydraulic jump, and open-channel flow, among others. Many numerical schemes have been developed in the past decades for the above equations (see [2, 3, 6, 7, 10, 14, 15, 19, 22] and references therein).

The shallow-water equations in lD case can be written as

$$W_t + F(W)_x = S, \tag{1.1}$$

where $W = (h, hU)^T$ is the vector of flow variables and $F(W) = (hU, hU^2 + \frac{1}{2}Gh^2)^T$ is the corresponding flux. In the above equations, $h$ is the water depth and $U$ is the water velocity. The source term has the form $S(W) = (0, -hGB'(x))^T$, which accounts for the dynamical effect on the fluid motion from the gravitational force and variable river bottom,

[1] Fax: (852)2358-1643.



0021-9991/02 $35.00

and $B(x)$ is the shape of the bed profile. If we integrate the above equation against $dx$ in a spatial element $j$ from $x_{j-1/2}$ to $x_{j+1/2}$, and $dt$ in a time interval from $t^n$ to $t^{n+1}$,

$$\int_{t^n}^{t^{n+1}} \int_{x_{j-1/2}}^{x_{j+1/2}} (W_t + F(W)_x)\, dx\, dt = \int_{t^n}^{t^{n+1}} \int_{x_{j-1/2}}^{x_{j+1/2}} S(W)\, dx\, dt,$$

we get

$$W_j^{n+1} - W_j^n = \frac{1}{\Delta x} \int_{t^n}^{t^{n+1}} \big(F_{j-1/2}(t) - F_{j+1/2}(t)\big)\, dt + \frac{1}{\Delta x} \int_{x_{j-1/2}}^{x_{j+1/2}} \int_{t^n}^{t^{n+1}} S(W)\, dx\, dt, \tag{1.2}$$

where $\Delta x = x_{j+1/2} - x_{j-1/2}$ is the cell size and $W_j$ is the averaged value of $W$ in cell $j$, i.e.,

$$W_j = \frac{1}{\Delta x} \int_{x_{j-1/2}}^{x_{j+1/2}} W\, dx.$$

The above equation is an integral form of Eq. (1.1), which is exact and equivalent to Eq. (1.1). Physically, Eq. (1.2) reflects the following fact. The second term on the right hand side describes the gravitational effect on a fluid element moving from one place to another place within the same cell due to the nonsmoothness of the river bottom. If the fluid element passes through the cell interface, its contribution is included in the first term on the right hand side of Eq. (1.2), i.e., the so-called cell interface flux. Since the fluid particle should have no idea about the location of the cell interface, the nonsmoothness of the river bottom and the gravitational force will equally take effect on any fluid element moving inside the same cell or passing through the cell interface within a numerical time step. Therefore, a physical flux function at a cell interface should include the source term influence too, such as the fluid acceleration or deceleration due to river topography when going through the cell boundary. This is one of the main points we would like to address in the current paper.

Since different shapes of the river bottom have different dynamical influence on the fluid motion, in order to get an accurate solution based on Eq. (1.2), we need to discretize the river bottom $B(x)$ first. In a first-order approximation, the river bottom can be approximated as flat inside each cell (see Fig. 1), then Eq. (1.2) becomes

$$W_j^{n+1} - W_j^n = \frac{1}{\Delta x} \int_{t^n}^{t^{n+1}} \big(F_{j-1/2}^+(t) - F_{j+1/2}^-(t)\big)\, dt, \tag{1.3}$$

where $-$ and $+$ mean the left and right sides of a cell interface.

The absence of the explicit source term in the above equation is due to the flat bottom $B'(x) = 0$ inside each cell. But the flux in the above equations should be based not only on the flow variables $W_j$ and $W_{j+1}$ but also on the bottom height jump from $B_j$ to $B_{j+1}$. A Riemann solution based on the above initial condition has been obtained by a few authors [1, 8, 15] (see [16] also). A similar idea has been applied to other equations with different source terms [11]. Under the condition shown in Fig. 1, due to the bottom jump the momentum flux will not be a continuous function at the cell interface. In other words, the momentum lost in cell $j$ at $x_{j+1/2}$ is not equal to the momentum received in cell $j+1$. The reason is that when the fluid passess through the cell interface, it has to overcome the gravitational barrier, where the kinetic and potential energy exchange takes place. Under the assumption

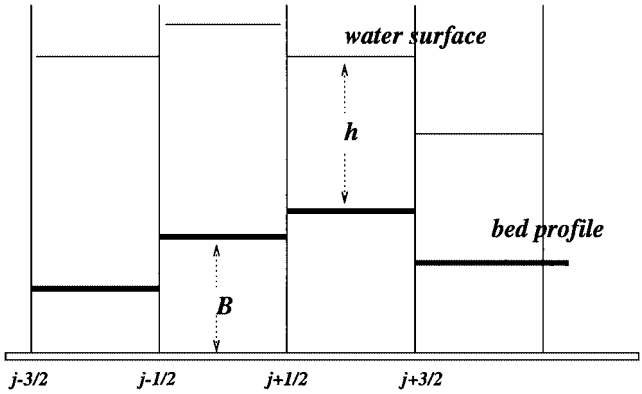


**FIG. 1.** First-order discretization of the river bottom. Due to bottom jump at the cell interface, the momentum flux is not continuous there.

of stationary step transition (SST) at the cell interface, there are about 20 cases with different wave patterns in the above exact Riemann problem, and the solution itself can be hardly used in any practical flow applications [1]. In contrast, in hydraulics engineering an empirical local head loss due to sudden channel geometry change is used to simulate the momentum flux discontinuity [5].

Since we have the freedom to choose the location of a cell interface, an alternative choice is to shift its location by a half cell size (see Fig. 2). In this case, Eq. (1.2) becomes

$$W_j^{n+1} - W_j^n = \frac{1}{\Delta x}\int_{t^n}^{t^{n+1}} \big(F_{j-1/2}(t) - F_{j+1/2}(t)\big)dt + \frac{1}{\Delta x}\int_{x_{j-1/2}}^{x_{j+1/2}}\int_{t^n}^{t^{n+1}} S(W)\,dx\,dt.$$

In the above equation, the source term effect can be ignored in the flux evaluation because of the zero river bottom slope around the cell interface, but the integration of the source term inside each cell becomes complicated due to the river bed jump. A solution which accounts for this kind of source term effect inside each cell is obtained by LeVeque using a quasisteady approximation [14], which is similar to the SST assumption. LeVeque's scheme

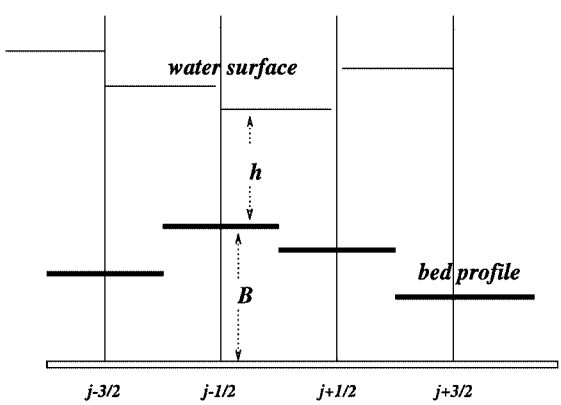


**FIG. 2.** With the shift of the cell interface, the source term effect needs to be accounted for inside each cell.

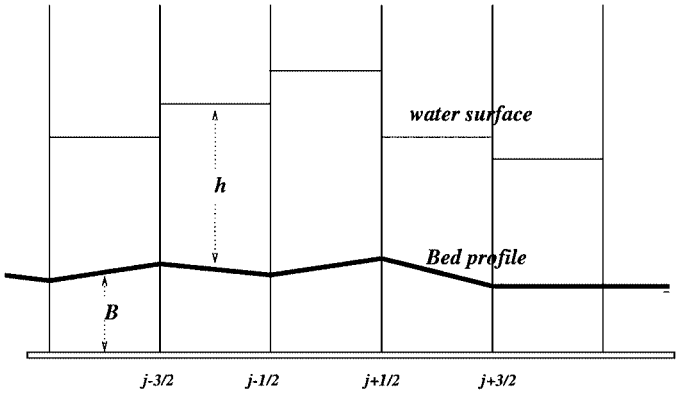


**FIG. 3.** Second-order discretization of the river bottom. The bottom profile inside each cell has a linear distribution.

gives excellent results in many quasisteady sound wave propagation cases, which will add difficulties to simple operator splitting schemes. Also, due to the quasisteady approximation, LeVeque has noticed the difficulties of his scheme in the application to the unsteady flow with shock waves.

In a second-order approximation of the river bottom, the bed shape can be approximated as a linear function inside each cell (see Fig. 3). As a special case, in order to develop a well-balanced scheme, which is defined as a scheme to keep the solution $U = 0, h + B =$ constant exactly (see Fig. 4), the flux and source terms in Eq. (1.2) have to be precisely matched,

$$\frac{1}{\Delta x}\int_{t^n}^{t^{n+1}} \big(F_{j-1/2}(t) - F_{j+1/2}(t)\big)\,dt = -\frac{1}{\Delta x}\int_{x_{j-1/2}}^{x_{j+1/2}}\int_{t^n}^{t^{n+1}} S_j(W)\,dx\,dt. \qquad (1.4)$$

Many well-balanced schemes have been obtained based on the above equation. For example, if the flux function is evaluated from the homogeneous hyperbolic system (without including

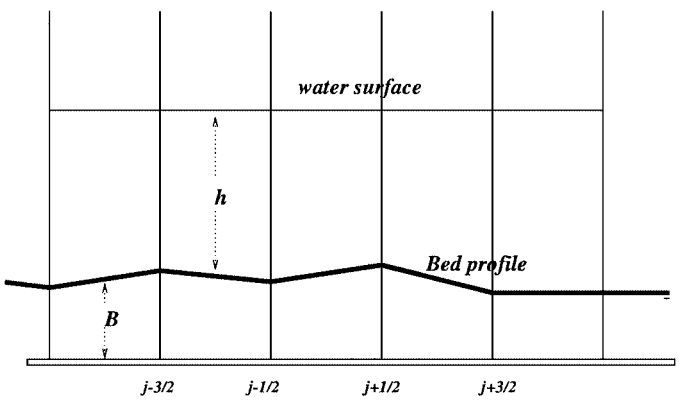


**FIG. 4.** An exact solution of the shallow water equations with source term, where $h + B =$ constant and $U = 0$.

a source term effect), the only way to keep the above equality is to deal with the source term, such as splitting it according to different wave modeling in the Riemann solution (see [3, 7, 10] and references therein), or using the cell interface flow variables of the Riemann solution to approximate the source term integration inside each cell [9, 12].

Recently, Zhou *et al*. developed a robust and well-balanced scheme based on the HLL Riemann solver and the surface gradient method (SGM) for initial data interpolation [22]. The merit of their approach is that their initial reconstruction is based on $h + B$ instead of $h$. Therefore, the equilibrium initial data $U = 0$ and $h + B =$ constant can be precisely kept after reconstruction. For example, in the case shown in Fig. 4, the water surface is still flat after data reconstruction and the flux function instantaneously at each cell interface is the pressure contribution $Gh_{j+1/2}^2/2$, which can be used to balance the source term effect exactly for each cell,

$$\frac{1}{2}G\left(h_{j+1/2}^2 - h_{j-1/2}^2\right) = -Gh_j\left(B_{j+1/2} - B_{j-1/2}\right). \tag{1.5}$$

So the equality in Eq. (1.4) holds. Even for the second-order SGM with the implementation of the Hancock technique, due to the independent time evolution for the left and right states at a cell interface the fluid distribution at the middle of a time step $t^{n+1/2}$ still has the distribution profile, shown in Fig. 4. Therefore, Eq. (1.5) is still correct. From this example, we may get an illusion that the inclusion of the source term in the flux evaluation may not be necessary. However, if we look careful at the initial data in Fig. 4, the $h$ and $B$ distributions around a cell interface should look like that in Fig. 5, where there are different slopes for both $h$ and $B$. The fortunate point in the method of Zhou *et al*. is that only the pointwise flow variables exactly at the cell interface $x_{j+1/2}$ and time $t = 0$ are used in the flux evaluation (like most other Riemann solvers). However, for a highly accurate scheme under the initial conditions of Fig. 5, if different slopes of $h$ anticipate the gas evolution (physically they really do), such as the case in the generalized Riemann solver, the solution from solving the homogeneous equations $W_t + F_x = 0$ will present a time-dependent flux function $F_{j+1/2}$, which is different from the purely pressure contribution $(1/2)Gh_{j+1/2}^2$ in Eq. (1.5). So in

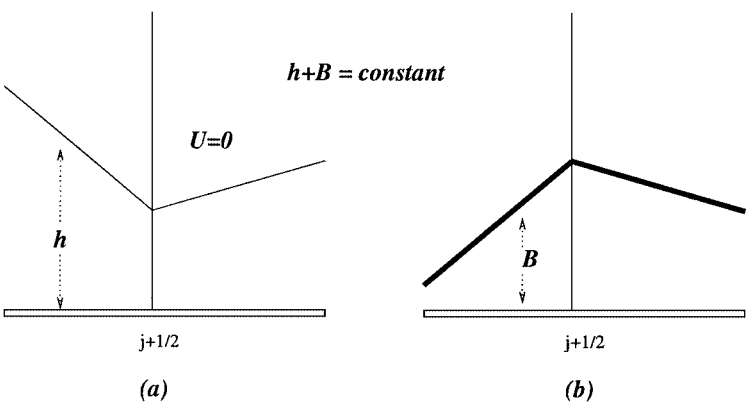


**FIG. 5.** The initial condition of $h$, $U$, and $B$ around a cell interface for the exact solution shown in Fig. 4. For a well-balanced scheme, the contribution to the flux function from the variable $h$ and $B$ distributions should be balanced exactly to have a final flux with a pressure contribution only at the cell interface.

order to keep Eq. (1.5) true in a high-order scheme with the inclusion of different initial $h$ slopes, as in Fig. 5, the source term effect has to be included as well in the flux evaluation. For a well-balanced scheme, the source term contribution from different $B$ slopes should precisely balance the effect from different $h$ slopes in this special case.

In terms of gas-kinetic schemes for the shallow-water equations, a fractional-step method is obtained in [6]. Since the source term is not included in the flux evaluation, the BGK scheme presented in [6] is not a well-balanced scheme, and it cannot keep the equilibrium state $U = 0$ and $h + B =$ constant exactly. Slyz and Prendergast [17] have extended the gas-kinetic BGK scheme to the Euler fluid under gravitational field. They also used a fractional-step method, where the flux evaluation is based on the homogeneous Euler equations. As analyzed in [17], the reason for them to ignore the gravitational force effect on the flux evaluation is that the gravitational force has only a higher order effect on the particle trajectory, such that $x = x' + u'(t - t') + \Phi_x(t - t')^2$, where the gravitational term is proportional to $(t - t')^2$. For a scheme with second-order accuracy in time, i.e., the gas evolution being proportional to $t$, the higher order term can be ignored. However, as pointed out in the current paper, the above analysis is incomplete. It is true that the gravitational force $\Phi_x$ has a second-order effect on the particle trajectory, but it has a first-order effect on the particle velocity $u = u' + \Phi_x(t - t')$. Due to the gravitational force, the change of particle velocity has a direct impact on the variation of the gas distribution function. Its contribution to the fluid motion is on the same order as those from the linear spatial variation of the flow variables, such as the water height or velocity gradients. Recently, Audusse *et al*. developed a first-order kinetic flux vector splitting scheme based on the collisionless Boltzmann equation for the shallow-water equations with source term [2]. With the appropriate choice of the flux splitting, their scheme is a well-balanced one to keep $U = 0$ and $h + B =$ constant. But the accuracy of this scheme to the problems, such as LeVeque's sound wave propagation tests, needs further investigation.

In order to develop an accurate and reliable scheme, the fluid physics has to be followed as closely as possible. For the shallow-water equations, the reality is that the source term does effect the fluid evolution around a cell interface and changes the numerical fluxes. The current paper presents such a scheme, where a time-dependent flux function is obtained by solving the gas-kinetic BGK model for the linearly distributed initial flow variables and bed profile around a cell interface (see Fig. 6). In the special case of Fig. 5, the current scheme could keep the exact solution of $U = 0$ and $h + B =$ constant, even in the 2D cases.

## 2. A BGK SCHEME FOR THE SHALLOW-WATER EQUATIONS

We consider the shallow-water equations with source term:

$$\begin{pmatrix} h \\ hU \end{pmatrix}_t + \begin{pmatrix} hU \\ hU^2 + \frac{1}{2}Gh^2 \end{pmatrix}_x = \begin{pmatrix} 0 \\ -B'(x)Gh \end{pmatrix}. \tag{2.6}$$

In this system, $h$ is the water height, $U$ the velocity, and $G$ the gravitational constant. $B(x)$ is the topology of the river bottom. The numerical discretization of the above equation with $W = (h, hU)^T$ is

$$W_j^{n+1} - W_j^n = \frac{1}{\Delta x}\int_{t^n}^{t^{n+1}} \left(F_{j-1/2}(t) - F_{j+1/2}(t)\right) dt + \frac{1}{\Delta x}\int_{x_{j-1/2}}^{x_{j+1/2}}\int_{t^n}^{t^{n+1}} S(W)\, dx\, dt.$$

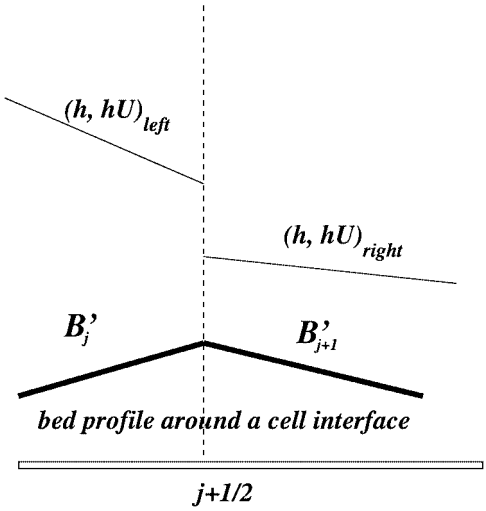


**FIG. 6.** The initial condition for the gas-kinetic BGK scheme. A time-dependent flux is obtained with the inclusion of both linearly distributed initial flow variables and the river bed slopes.

In the current study the source term in the momentum equation is always discretized as

$$\frac{1}{\Delta x}\int_{x_{j-1/2}}^{x_{j+1/2}}\int_{t^n}^{t^{n+1}} -B'(x)Gh\,dx\,dt = -\Delta t\,\frac{\left(h_j^n + h_j^{n+1}\right)}{2}B'(x_j)G,$$

where $B'(x_j)$ is the bed slope at the center of cell $j$. The scheme presented in this section is about the construction of a time-dependent numerical fluxes $F_{j+1/2}(t)$ under the general initial condition of Fig. 6 by solving the gas-kinetic BGK model [4].

The generalized BGK model with the inclusion of the gravitational force can be written as

$$f_t + uf_x + \Phi_x f_u = \frac{g-f}{\tau}, \tag{2.7}$$

where $f$ is the gas distribution function and $g$ the equilibrium state $f$ approaches. $\tau$ is the particle collision time and $\Phi_x$ is the gravitational acceleration due to the variable river bottom $\Phi_x = -GB'(x)$.

For the shallow-water equations, $f$ and $g$ are functions of space $x$, time $t$, and particle velocity $u$. The equilibrium state $g$ which maximizes the entropy for the shallow-water system is a Maxwellian distribution [6],

$$g = h\left(\frac{\lambda}{\pi}\right)^{\frac{1}{2}} e^{-\lambda(u-U)^2},$$

where $\lambda$ is defined by $\lambda = 1/(hG)$. Due to the conservation property in particle collisions, $f$ and $g$ satisfy the compatibility condition

$$\int (f-g)\psi_\alpha\,du = 0 \quad \text{for } \psi_\alpha = (1,u)^T, \tag{2.8}$$

at any point in space and time.

The integral solution of the BGK model is

$$f\left(x_{j+1/2}, t, u\right) = \frac{1}{\tau}\int_0^t g(x', t', u')e^{-(t-t')/\tau}\,dt' + e^{-t/\tau} f_0(x_0, u_0), \tag{2.9}$$

where $x_{j+1/2}$ is the location of the cell interface and $x_{j+1/2} = x' + u'(t-t') + \frac{1}{2}\Phi_x(t-t')^2$ is the particle trajectory. Also, due to the gravitational force, the particle velocity will change according to Newton's law $u = u' + \Phi_x(t-t')$. There are two unknowns in the above equation. One is the initial gas distribution function $f_0$ at time $t = 0$, and the other is the equilibrium state $g$ in both space and time locally around $(x_{j+1/2}, t = 0)$.

Before we construct the gas-kinetic scheme based on the above integral equation, let's first consider the particle velocity change due to the gravitational force and its modification to the gas distribution function. In the derivation below, terms on the order of $t^2$ are ignored automatically. Suppose that a particle is moving from $x'$ to $x$ in a short time interval $t - t'$. Because of the gravitational acceleration, the particle velocity will change from $u'$ to $u$ and their relation is $u = u' + \Phi_x(t-t')$. So due to the particle velocity change, an equilibrium state $g_0$ at time $t'$ can be expressed as

$$\begin{aligned} g_0 &= h\left(\frac{\lambda}{\pi}\right)^{\frac{1}{2}} e^{-\lambda(u'-U)^2} \\ &= h\left(\frac{\lambda}{\pi}\right)^{\frac{1}{2}} e^{-\lambda[(u-\Phi_x(t-t'))-U]^2} \\ &= h\left(\frac{\lambda}{\pi}\right)^{\frac{1}{2}} e^{-\lambda(u-U)^2} e^{2\lambda\Phi_x(u-U)(t-t')-\lambda\Phi_x^2(t-t')^2} \\ &= g e^{2\lambda\Phi_x(u-U)(t-t')-\lambda\Phi_x^2(t-t')^2}, \end{aligned}$$

where $g$ is the equilibrium state at time $t$. Note that in the above equation, only particle velocity change is accounted for. Using the Taylor expansion and neglecting $(t-t')^2$ order terms, the above equilibrium state can be approximated as

$$g_0 \simeq g[1 + 2\lambda\Phi_x(u-U)(t-t')].$$

The term $2\lambda\Phi_x(u-U)(t-t')g$ in the above equation presents the variation of the distribution function due to particle acceleration. Due to the Taylor expansion, the above equilibrium state $g_0$ deviates from an exact Maxwellian distribution. In order to compensate for the non-Maxwellian and the ignored higher order terms, we are going to put one additional constant, $\alpha$, in $\Phi_x$ term and express $g_0$ as

$$g_0 = g[1 + 2\alpha\lambda\Phi_x(u-U)(t-t')].$$

The value of $\alpha$ depends on the moments $(1, u, u^2)^T$ taken by the above distribution function. As analyzed later for a well-balanced scheme, $\alpha$ has to take the following constants for different moments,

$$\alpha_1 = 3/4, \quad \alpha_u = 1, \quad \alpha_{u^2} = 5/4.$$

The time evolution of the distribution function in space and time due to other factors, such as the velocity and water depth gradients, will be given later. The gravitational source term $\Phi_x$ under the condition of Fig. 6 can be written as

$$\Phi_x = -G\big(B'_j\big(1 - \mathrm{H}\big[x - x_{j+1/2}\big]\big) + B'_{j+1}\mathrm{H}\big[x - x_{j+1/2}\big]\big), \tag{2.10}$$

where $\mathrm{H}[x]$ is the Heaviside function, and $B'_j$ and $B'_{j+1}$ are the constant slopes in cell $j$ and $j+1$. The following is the numerical procedures to get the solution of Eq. (2.9).

*Step 1.* With the cell-averaged data $h_j$ and $h_jU_j$, we are going to use the surface gradient method (SGM) to get the initial data interpolation for the water height $h$ and momentum $hU$ [22]. In the SGM, the nonlinear limiter is used on the water surface height $\eta_j = h_j + B_j$ and the momentum $h_jU_j$. After the MUSCL-type interpolation, the flow distributions $W_j = (h_j, h_jU_j)^T$ around a cell interface $x_{j+1/2}$ can be described as

$$W_j(x) = W_j(x_j) + \frac{W_j\big(x_{j+1/2}\big) - W_j\big(x_{j-1/2}\big)}{x_{j+1/2} - x_{j-1/2}}\big(x - x_j\big) \quad \text{for } x \in \big[x_{j-1/2}, x_{j+1/2}\big], \tag{2.11}$$

where the water heights at the left and right hand sides of a cell interface $x_{j+1/2}$ are

$$h_j\big(x_{j+1/2}\big) = \eta_j\big(x_{j+1/2}\big) - B\big(x_{j+1/2}\big) \quad \text{and} \quad h_{j+1}\big(x_{j+1/2}\big) = \eta_{j+1}\big(x_{j+1/2}\big) - B\big(x_{j+1/2}\big).$$

There is a possible discontinuity between $W_j(x_{j+1/2})$ and $W_{j+1}(x_{j+1/2})$ (see Fig. 6).

*Step 2.* Based on the reconstructed data in Step 1, around each cell interface $x_{j+1/2}$ we can construct an initial gas distribution function $f_0$,[2]

$$\begin{aligned} f_0(x,u) = {} & g^l\big(1 + a^l\big(x - x_{j+1/2}\big)\big)\big(1 - H\big[x - x_{j+1/2}\big]\big) \\ & + g^r\big(1 + a^r\big(x - x_{j+1/2}\big)\big)\,\mathrm{H}\big[x - x_{j+1/2}\big], \end{aligned} \tag{2.12}$$

where the states $g^l$ and $g^r$ are the Maxwellian distribution functions which have the one-to-one correspondence with the conservative variables at the cell interface $x_{j+1/2}$,

$$g^l = g^l\big(W_j\big(x_{j+1/2}\big)\big) \quad \text{and} \quad g^r = g^r\big(W_{j+1}\big(x_{j+1/2}\big)\big).$$

For example, with the distribution

$$g^l = h^l\left(\frac{\lambda^l}{\pi}\right)^{\frac{1}{2}} e^{-\lambda^l(u-U^l)^2},$$

all coefficients in $g^l$ can be obtained as

$$\begin{pmatrix} h^l \\ U^l \\ \lambda^l \end{pmatrix} = \begin{pmatrix} h_j\big(x_{j+1/2}\big) \\ h_jU_j\big(x_{j+1/2}\big)/h_j\big(x_{j+1/2}\big) \\ 1/\big(Gh_j\big(x_{j+1/2}\big)\big) \end{pmatrix}.$$

[2] Since we are not solving viscous shallow-water equations, the nonequilibrium part in $f_0$, which contributes mostly to resolve the dissipative fluid structure, i.e., the shock structure, is ignored in the initial gas distribution function. For a viscous flow simulation, the distribution based on the Chapman–Enskog expansion needs to be used (see [21] for details).

Similar equations can be found for $g^r$. The parameters $a^{l,r}$ in Eq. (2.12) are from the Taylor expansion of a Maxwellian and have the form

$$a^{l,r} = m_1^{l,r} + m_2^{l,r}u + m_3^{l,r}u^2.$$

The coefficients $(m_1^{l,r}, m_2^{l,r}, m_3^{l,r})$ are determined from $(h^l, h^lU^l)$ and $(h^r, h^rU^r)$ and their initial slopes in cells $j$ and $j+1$,

$$\left(\frac{\partial h^l}{\partial x}, \frac{\partial (hU)^l}{\partial x}\right) \quad \text{and} \quad \left(\frac{\partial h^r}{\partial x}, \frac{\partial (hU)^r}{\partial x}\right).$$

The relations are

$$\begin{aligned} m_1^{l,r} &= \left[\left(\frac{1}{2h} + \frac{3U^2}{Gh^2}\right)\frac{\partial h}{\partial x} - \frac{2U}{Gh^2}\frac{\partial (hU)}{\partial x}\right]^{l,r}, \\ m_2^{l,r} &= \left[-\frac{4U}{Gh^2}\frac{\partial h}{\partial x} + \frac{2}{Gh^2}\frac{\partial (hU)}{\partial x}\right]^{l,r}, \\ m_3^{l,r} &= \left[\frac{1}{Gh^2}\frac{\partial h}{\partial x}\right]^{l,r}. \end{aligned} \tag{2.13}$$

So, all coefficients in Eq. (2.12) can be determined from the initially reconstructed data in Step 1. For simplification, we assume $x_{j+1/2} = 0$ in the rest of this paper.

Equation (2.12) shows the gas distribution function $f$ at time $t = 0$. When taking $f_0$ into the integral solution (2.9), we need to figure out the particle arriving $x = 0$ at time $t$ with velocity $u$,

$$\begin{aligned} f_0\left(-ut - \frac{1}{2}\Phi_x t^2, u - \Phi_x t\right) &= g_0^l\left(1 + a^l\left(-ut - \frac{1}{2}\Phi_x t^2\right)\right)\left(1 - H\left(-ut - \frac{1}{2}\Phi_x t^2\right)\right) \\ &\quad + g_0^r\left(1 + a^r\left(-ut - \frac{1}{2}\Phi_x t^2\right)\right)H\left(-ut - \frac{1}{2}\Phi_x t^2\right) \\ &\simeq g_0^l(1 - uta^l)H(u) + g_0^r(1 - uta^r)(1 - H(u)), \end{aligned}$$

where all terms proportional to $t^2$ have been ignored. The states $g_0^l$ and $g_0^r$ are different from the states $g^l$ and $g^r$ in Eq. (2.12) due to the particle velocity change from time $t = 0$ to $t$. The relations between $g_0^l$, $g_0^r$, $g^l$, and $g^r$ are

$$g_0^l = g^l(1 - 2\alpha\lambda^l\Phi_x(u - U^l)t)$$

and

$$g_0^r = g^r(1 - 2\alpha\lambda^r\Phi_x(u - U^r)t).$$

Therefore,

$$\begin{aligned} f_0\left(-ut - \frac{1}{2}\Phi_x t^2, u - \Phi_x t\right) &\simeq g^l(1 - 2\alpha\lambda^l\Phi_x(u - U^l)t)(1 - uta^l)\,H(u) \\ &\quad + g^r(1 - 2\alpha\lambda^r\Phi_x(u - U^r)t)(1 - uta^r)(1 - H(u)). \end{aligned}$$

We can further simplify the above expression to

$$f_0\left(-ut-\frac{1}{2}\Phi_x t^2, u-\Phi_x t\right) \simeq g^l(1+2\alpha\lambda^l G B'_j(u-U^l)t-uta^l)H(u) + g^r(1+2\alpha\lambda^r G B'_{j+1}(u-U^r)t-uta^r)(1-H(u)). \tag{2.14}$$

From the above equation, we can see that the gravitational froce contributes to the variation of the particle distribution function on the first order of time $t$, which is on the the same order as the contributions from terms $a^l$ and $a^r$. The claim that gravitational force has no first-order contribution ($\sim t$) to the expansion of a particle distribution function in [17] is inappropriate. Due to the characteristic line $x = x' + u'(t-t') + \frac{1}{2}\Phi_x(t-t')^2$ and $u = u' + \Phi_x(t-t')$ in the particle movement, the Heaviside function in $\Phi_x$ of Eq. (2.10) becomes approximately $\mathrm{H}[x'] = \mathrm{H}[-u(t-t')]$ at $(x=0, t)$. Since $t > t'$, the gravitational force term in Eq. (2.14) is replaced by

$$\Phi_x = -G(B'_j\mathrm{H}[u] + B'_{j+1}(1-\mathrm{H}[u])).$$

The physical meaning of the above equation is that in terms of the moving particles toward the cell interface (forming fluxes), the left bottom slope $B'_j$ will effect these particles with velocity $u > 0$ and the right slope $B'_{j+1}$ to the particles with velocity $u < 0$. Since the expansion is truncated to the order of $t$, those particles which pass the interface, then turn back (U-turn) in a short time $t - t'$, have been ignored in the above approximation.

*Step 3*. After constructing the initial state $f_0$, the equilibrium state $g$ is assumed to be continuous across a cell interface but with different slopes at the left and right hand sides,

$$g = g_0\big(1 + (1-\mathrm{H}[x])\bar{a}^l x + \mathrm{H}[x]\bar{a}^r x + \bar{A}t\big), \tag{2.15}$$

where $g_0$ is the equilibrium state located at $x = 0$ and $t = 0$,

$$g_0 = h_0\left(\frac{\lambda_0}{\pi}\right)^{\frac{1}{2}} e^{-\lambda_0(u-U_0)^2}.$$

Here $\bar{a}^l$, $\bar{a}^r$, and $\bar{A}$ in Eq. (2.15) have the forms

$$\begin{aligned} \bar{a}^{l,r} &= \bar{m}_1^{l,r} + \bar{m}_2^{l,r}u + \bar{m}_3^{l,r}u^2, \\ \bar{A} &= \bar{A}_1 + \bar{A}_2 u + \bar{A}_3 u^2. \end{aligned} \tag{2.16}$$

Taking both limits ($x \to 0, t \to 0$) in Eqs. (2.9) and (2.15), and applying the compatibility condition (2.8) at $(x = 0, t = 0)$, the macroscopic variables corresponding to $g_0$ can be uniquely determined in terms of $f_0$,

$$W_0 = \begin{pmatrix} h_0 \\ h_0U_0 \end{pmatrix} = \int g_0\psi_\alpha\, du = \int [g^l\mathrm{H}(u) + g^r(1-\mathrm{H}(u))]\psi_\alpha\, du, \tag{2.17}$$

where $W_0$ is the "averaged" flow variables at the cell interface. Then, connecting $W_0$ to the cell-centered values $W_j(x_j)$ and $W_{j+1}(x_{j+1})$, we can get two slopes for mass and momentum separately,

$$\begin{aligned}\left(\frac{\partial h_0^l}{\partial x}, \frac{\partial (hU)_0^l}{\partial x}\right)^T &= \frac{W_0 - W_j(x_j)}{x_{j+1/2} - x_j} \qquad \text{for } x \le 0,\\ \left(\frac{\partial h_0^r}{\partial x}, \frac{\partial (hU)_0^r}{\partial x}\right)^T &= \frac{W_{j+1}(x_{j+1}) - W_0}{x_{j+1} - x_{j+1/2}} \quad \text{for } x \ge 0,\end{aligned} \tag{2.18}$$

from which $(\bar{a}^l, \bar{a}^r)$ can be determined in a way similar to that shown in Eq. (2.13). Now, the unknown in Eq. (2.15) is $\bar{A}$, which can be expressed as

$$\begin{aligned}\bar{A}_1 &= \left(\frac{1}{2h_0} + \frac{3U_0^2}{Gh_0^2}\right)\frac{\partial h_0}{\partial t} - \frac{2U_0}{Gh_0^2}\frac{\partial (hU)_0}{\partial t},\\ \bar{A}_2 &= -\frac{4U_0}{Gh_0^2}\frac{\partial h_0}{\partial t} + \frac{2}{Gh_0^2}\frac{\partial (hU)_0}{\partial t},\\ \bar{A}_3 &= \frac{1}{Gh_0^2}\frac{\partial h_0}{\partial t},\end{aligned} \tag{2.19}$$

where $\partial h_0/\partial t$ and $\partial (hU)_0/\partial t$ need to be determined. In the above equilibrium state $g$, we do not include the gravitational force effect to the particle velocity change. This effect will be included in the integral solution (2.9) in the following way. For an equilibrium state $g(x', t', u')$ at $x'$ and $t'$, its particle will get to $x = 0$ at time $t - t'$. In this particle transport process, the particle velocity $u'$ will be changed from $u'$ to $u$ through the relation $u = u' + \Phi_x(t - t')$. With the inclusion of the gravitational force effect during the time interval $(t - t')$, the integration of $g(x', t', u')$ in Eq. (2.9) becomes

$$\begin{aligned}\int_0^t g(x', t', u') e^{-(t-t')/\tau}\, dt' = \int_0^t g_0 [1 - u(t - t')(\bar{a}^l \mathrm{H}[u] + \bar{a}^r (1 - \mathrm{H}[u]))\\ + \bar{A}t' - 2\alpha\lambda_0 \Phi_x (u - U_0)(t - t')] e^{-(t-t')/\tau}\, dt',\end{aligned} \tag{2.20}$$

where the particle velocity change has been included. Due to the integration on the characteristic line $x = x' + u'(t - t')$, $\Phi_x$ in the above equation has the form

$$\Phi_x = -G(B_j' \mathrm{H}[u] + B_{j+1}'(1 - \mathrm{H}[u])).$$

*Step 4.* Substituting Eqs. (2.14) and (2.20) into the integral solution (2.9), we can obtain the distribution function $f$ at $x = 0$,

$$\begin{aligned}f(0, t, u) = \gamma_0 g_0 + \gamma_1 [(\bar{a}^l \mathrm{H}[u] + \bar{a}^r (1 - \mathrm{H}[u]))u - 2\alpha\lambda_0 G(B_j' \mathrm{H}[u]\\ + B_{j+1}'(1 - \mathrm{H}[u]))(u - U_0)\big] g_0 + \gamma_2 \bar{A} g_0 + \gamma_3 (\mathrm{H}[u] g^l\\ + (1 - \mathrm{H}[u]) g^r) + \gamma_3 [-t(ua^l - 2\alpha\lambda^l G B_j'(u - U^l))\mathrm{H}[u] g^l\\ - t(ua^r - 2\alpha\lambda^r G B_{j+1}'(u - U^r))(1 - \mathrm{H}[u]) g^r],\end{aligned} \tag{2.21}$$

where

$$\gamma_0 = 1 - e^{-t/\tau},$$
$$\gamma_1 = \tau\left(-1 + e^{-t/\tau}\right) + te^{-t/\tau},$$
$$\gamma_2 = \tau\left(t/\tau - 1 + e^{-t/\tau}\right),$$
$$\gamma_3 = e^{-t/\tau}.$$

As pointed out earlier, there are two unknowns $(\partial h_0/\partial t, \partial(hU)_0/\partial t)$ in $\bar{A}$ of Eq. (2.21). Since the compatibility condition must be satisfied everywhere in space and time, it can be integrated in a whole CFL time step $\Delta t$ at $x = 0$,

$$\int_0^{\Delta t} \int (f(0,t,u) - g(0,t,u))\psi_\alpha \, dt \, du = 0, \tag{2.22}$$

from which we have

$$\begin{aligned}\left(\frac{\partial h_0}{\partial t}, \frac{\partial (hU)_0}{\partial t}\right)^T = \int \big[&\Gamma_1(\bar{a}^l \mathrm{H}[u] + \bar{a}^r(1 - \mathrm{H}[u]))ug_0 - \Gamma_1(B'_j \mathrm{H}[u] \\ &+ B'_{j+1}(1 - \mathrm{H}[u]))2\alpha\lambda_0 G(u - U_0)g_0 + \Gamma_2(a^l u \mathrm{H}[u] g^l \\ &+ a^r u(1 - \mathrm{H}[u])g^r) - \Gamma_2(2\alpha\lambda^l(u - U^l)B'_j \mathrm{H}[u]g^l \\ &+ 2\alpha\lambda^r(u - U^r)B'_{j+1}(1 - \mathrm{H}[u])g^r)\big]\psi_\alpha \, du. \end{aligned} \tag{2.23}$$

All terms on the right hand side of the above equation are known and

$$\Gamma_0 = \Delta t - \tau\left(1 - e^{-\Delta t/\tau}\right),$$
$$\Gamma_1 = \left(-\Delta t + 2\tau\left(1 - e^{-\Delta t/\tau}\right) - \Delta t e^{-\Delta t/\tau}\right)/\Gamma_0,$$
$$\Gamma_2 = \left(\Delta t e^{-\Delta t/\tau} - \tau\left(1 - e^{-\Delta t/\tau}\right)\right)/\Gamma_0.$$

So, $\bar{A}$ in Eq. (2.16) is totally determined.

*Step 5*. The time-dependent numerical fluxes of mass and momentum across the cell interface can be obtained by integrating Eq. (2.21),

$$\begin{pmatrix} F_h(t) \\ F_{hU}(t) \end{pmatrix}_{j+1/2} = \int u \begin{pmatrix} 1 \\ u \end{pmatrix} f_{j+1/2}(0,t,u) \, du. \tag{2.24}$$

In the above distribution function $f$, the parameters $\alpha_1$, $\alpha_u$, and $\alpha_{u^2}$ are determined by applying the scheme to the exact solution of the shallow water equations, i.e., $U = 0$ and $h_j + B_j =$ constant. In this equilibrium case, the above flux function in Eq. (2.24) should have the constant pressure contribution only, such as $(F_h(t) = 0, F_{hU}(t) = Gh^2_{j+1/2}(0)/2)$ at a cell interface. Therefore, in this case the gravitational contribution due to the bottom slope,

$$-\int \psi_\alpha 2\alpha\lambda G B' u g \, du,$$

needs to be exactly balanced by the contribution from water-height variation,

$$\int \psi_\alpha a u g \, du = \int \psi_\alpha((1/2h)\partial h/\partial x + (u^2/Gh^2)\partial h/\partial x)ug \, du,$$

(see Eq. (2.13) for $a$ term in the equilibrium case) for all terms from both $f_0$ and $g$ in Eq. (2.21). Then, the coefficient $\alpha$ have the values $\alpha_1 = 3/4, \alpha_u = 1, \alpha_{u^2} = 5/4$ when taking different moments $\psi_\alpha = (1, u, u^2)^T$. Therefore, even with different slopes of $h$ and $B$ on both sides of a cell interface, the kinetic scheme will keep the exact equilibrium solution shown in Fig. 4. In other words, the gas-kinetic BGK scheme is a well-balanced method. Later, we can see that the BGK scheme will also keep the equilibrium solution in the 2D case to the accuracy of machine zero. For unsteady, transcritical, and all other flow computations, the same constant coefficients ($\alpha_i, i = 1, u, u^2$) are used. For nonstationary solutions, it seems that there is no any sensitive dependence on the choices of these parameters. For example, for strongly unsteady flow, the ignoring of the whole source term effect in the flux function may have no much impact on the solution. But for the quasisteady flows, any change of the above parameters will deteriorate the solutions.

For most engineering applications, if the efficiency is the main concern, the above BGK scheme can be much simplified by removing particle collisional term. The gas distribution function based on the collisionless Boltzmann equation becomes

$$\begin{aligned} f(0,t,u) = {} & (\mathrm{H}[u]g^l + (1-\mathrm{H}[u])g^r) + [-t(ua^l - 2\alpha\lambda^l G B'_j(u-U^l))\mathrm{H}[u]g^l \\ & - t(ua^r - 2\alpha\lambda^r G B'_{j+1}(u-U^r))(1-\mathrm{H}[u])g^r], \end{aligned} \tag{2.25}$$

and the numerical flux can be evaluated similarly as Eq. (2.24) by using the above $f$. This scheme is called the kinetic flux vector splitting (KFVS) method, which has a close relation to the flux vector splitting scheme. The above simplified scheme is also a well-balanced method for keeping the steady state $U = 0$ and $h + B =$ constant exactly. It works for all test case shown in the next section except it is more dissipative in the simulation results. The dissipation in the above simplified scheme is on the same order as other flux vector splitting (FVS) schemes or the HLL method. Since we are not solving the viscous shallow-water equations, additional dissipation seems not be so harmful. Since the particle motion is much simpler than the propagation of waves, it is not surprising that a well-balanced kinetic scheme can be developed easily in comparison with the schemes based on the macroscopic equations. With the incorporation of all slopes of $h$, $hU$, and $B$ in the evaluation of the distribution function $f$ in Eq. (2.25), it is different from the kinetic approach in [2], even through they are based on solving the same collisionless Boltzmann equation. With the capturing of particle accelerating or decelerating mechanisms in the flux evaluation of the kinetic BGK scheme, the BGK current method should be a physically reliable one. The implementation of other physical terms in it for the complicated wave phenomena, such as resonance [15], bed friction [22], and roll waves problems [13], will be investigated in the near future.

## 3. NUMERICAL EXAMPLES

In this section, we test the gas-kinetic BGK scheme in many test cases. In all calculations, the collision time $\tau$ takes the values

$$\tau = C_1 \Delta t + C_2 \Delta t \frac{|h^l h^l - h^r h^r|}{h^l h^l + h^r h^r}, \tag{3.26}$$

where $C_1 = 0.05, C_2 = 1.0$. As analyzed previously for the compressible Euler and Navier–Stokes equations, usually the first term on the right hand side of $\tau$ is related to the physical

viscosity coefficient and the second one is used to provide the numerical dissipation needed in the underresolved flow region. Since all test cases in this section are targeted to the inviscid shallow-water equations, the physical viscous term is replaced by a numerical value. Due to the inclusion of the particle collisional term in the BGK model, the current scheme has less dissipation than the KFVS scheme based on the collisionless Boltzmann equation. In all calculations, the time step $\Delta t$ is determined from the CFL condition, and different CFL numbers, such as 0.1, 0.5, and 0.8, have been tested. The simulation results are basically not sensitive to these changes. As pointed out earlier, all initial interpolations are based on the van Leer limiter. The gravitational constant $G$ takes the value 9.8 or the value explicitly given.

*Case 1.* Here we test two standard shock tube problems, where the homogeneous shallow-water equations are solved. The initial condition for the first example is

$$(h_l = 1.0, U_l = 0.0)|_{x<0.5} \quad \text{and} \quad (h_r = 0.1, U_r = 0.0)|_{x\geq 0.5}.$$

The simulation results $h$ and $hU$ with 100 grid points at the output time $t = 0.3$ are shown in Figs. 7 and 8, where the solid lines are the exact solutions. This test shows the good shock-capturing ability of the gas-kinetic BGK scheme. In the second example, we consider the shallow-water solution with two strong rarefaction waves. The initial condition is

$$(h_l = 1.0, U_l = -0.5)|_{x<0.5} \quad \text{and} \quad (h_r = 0.1, U_r = 0.5)|_{x\geq 0.5}.$$

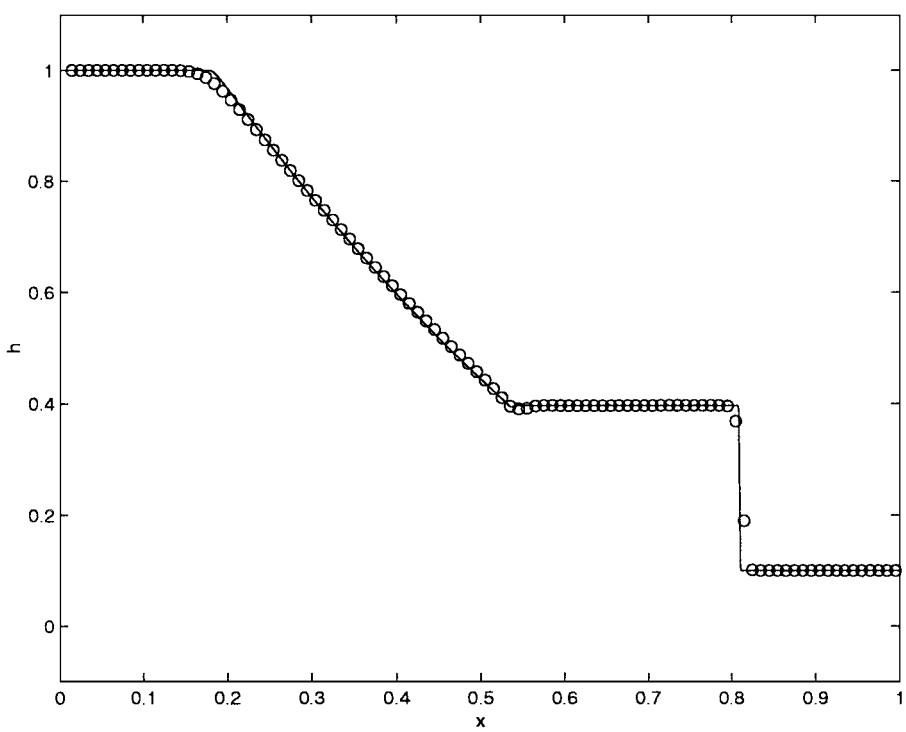


**FIG. 7.** The BGK solution of a shock tube problem with flat river bottom. The homogeneous shallow-water equations are solved. Water height is presented and the cell size is $\Delta x = 1/100$.

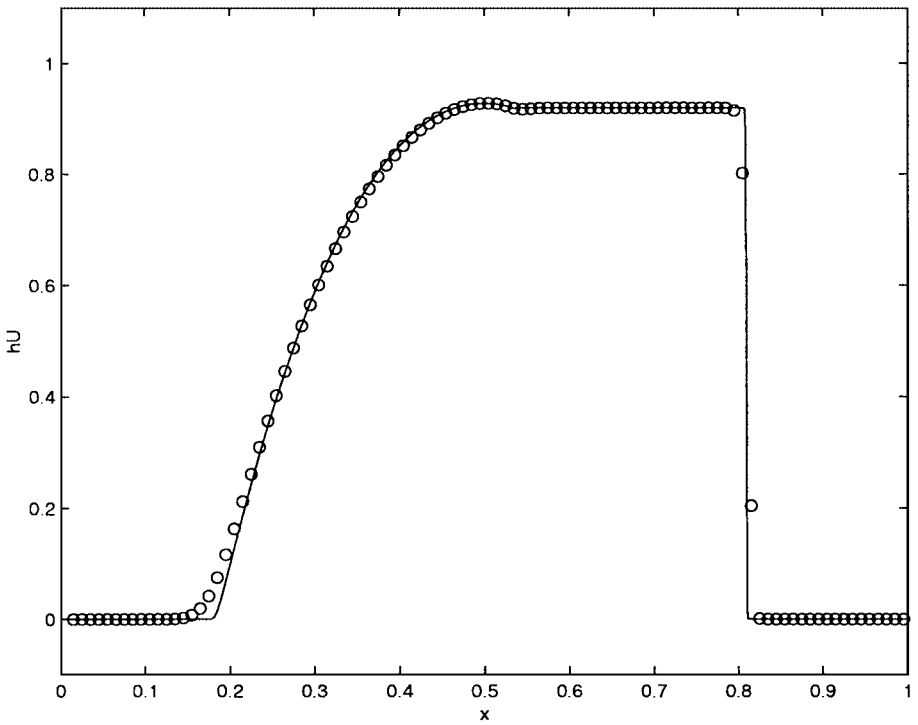


**FIG. 8.** Continuation of Fig. 7. Momentum distribution.

The simulation results $h$ and $U$ with 100 grid points at the output time $t = 2.5$ are shown in Figs. 9 and 10, where the solid lines are the exact solutions. As pointed out by Toro [18], most upwinding schemes could fail in this test. The Godunov method with an exact Riemann solution needs a dry-bed condition to pass this test; even the exact solution for this problem has not gotten to the dry condition (vacuum) yet. The BGK scheme can pass this test without any difficulty.

*Case 2*. This is a steady state case to check both the dissipative and dispersive errors in the kinetic scheme. The bottom shape of the river has the form

$$B(x) = 0.2e^{-(x+1)^2/2} + 0.3e^{-(x-1.5)^2}.$$

The computational domain is in the range $x \in [-10, 10]$, and the left boundary condition is $U_- = 1.0$, $h_- = 1.0$. The equilibrium state can be obtained exactly for this problem (see Fig. 11). The numerical solutions $U$ and $h + B$ obtained with 100 and 50 grid points are shown in Fig. 12. Even with the coarse mesh, such as $\Delta x = 0.4$, accurate solutions can be obtained.

*Case 3*. This is an unsteady test problem proposed by Bermudez and Vazquez [3]. The bed topography is defined by

$$B(x) = 10 + \frac{40x}{L} + 10 \sin\left[\pi\left(\frac{4x}{L} - \frac{1}{2}\right)\right],$$

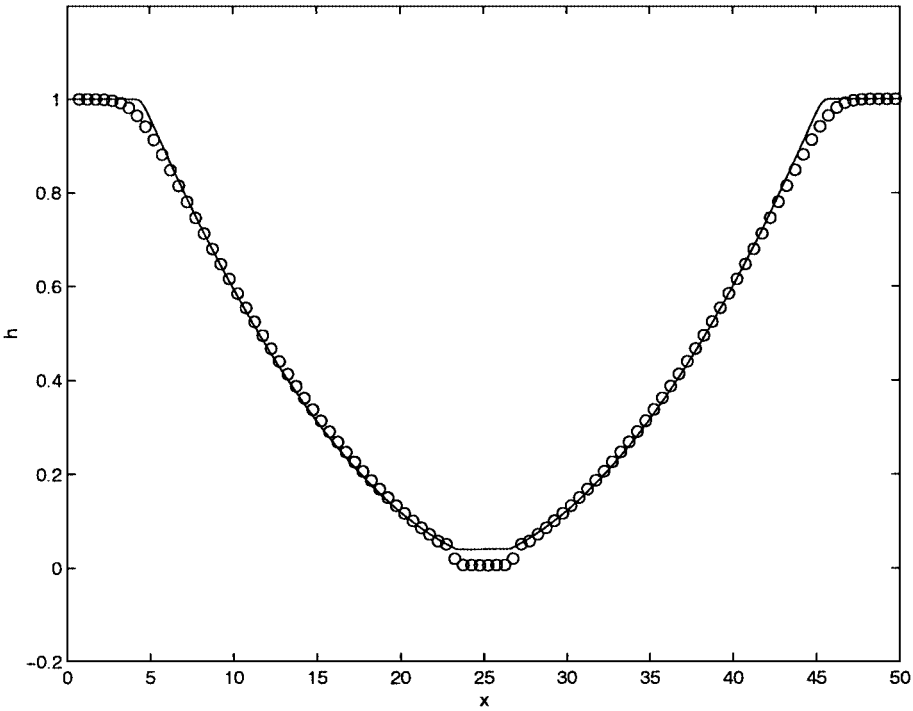


**FIG. 9.** The BGK solution for the shock tube problem with two rarefaction waves. The cell size used is $\Delta x = 0.5$. Water height $h$ is presented and the solid line is the exact solution.

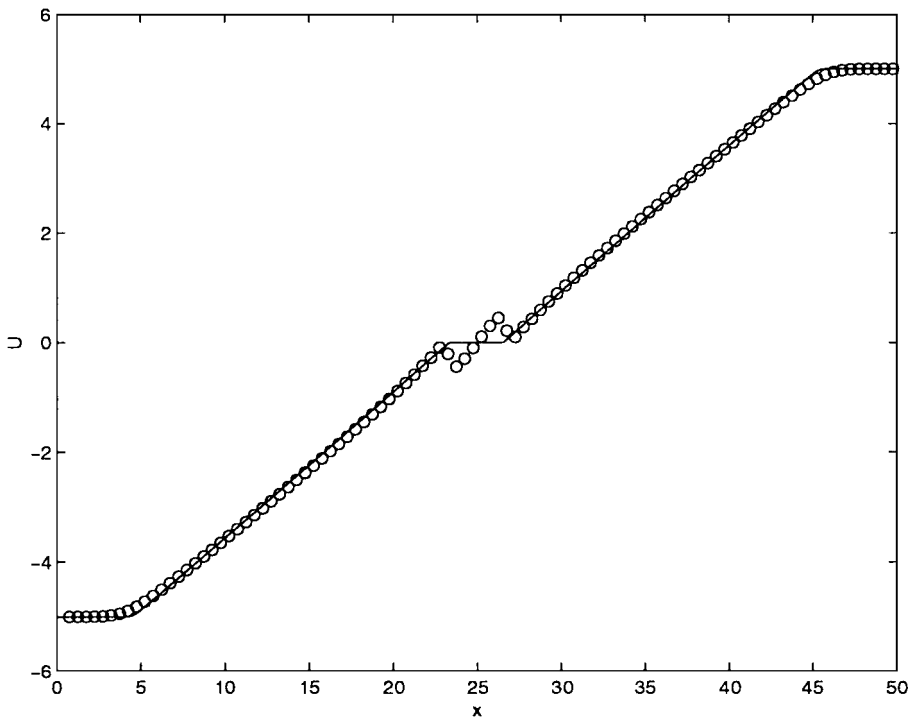


**FIG. 10.** Continuation of Fig. 9. Velocity distribution.

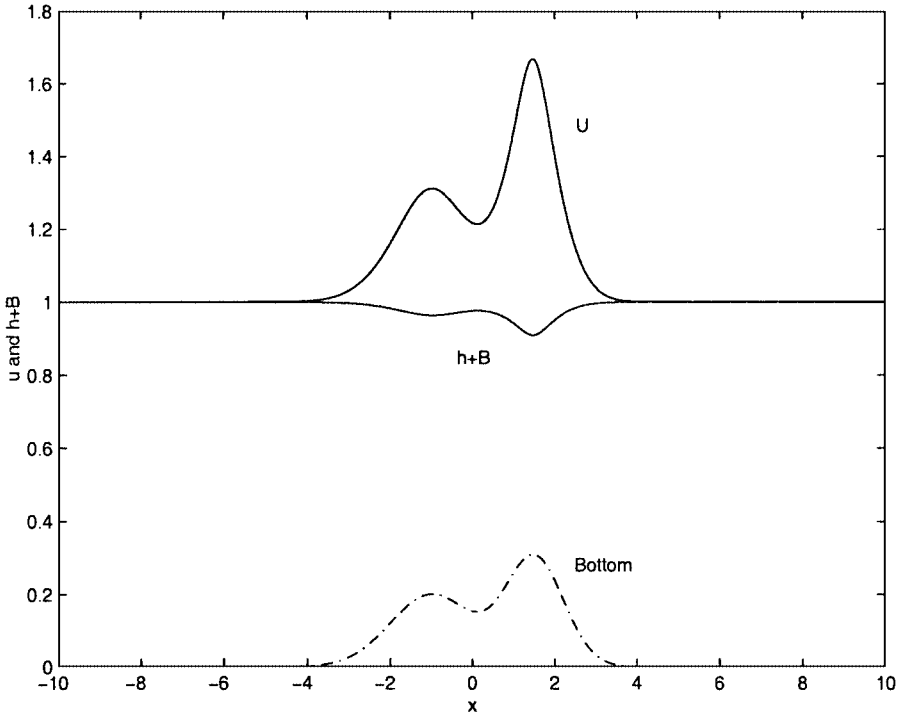


**FIG. 11.** River bottom and exact steady state solutions for Case 2.

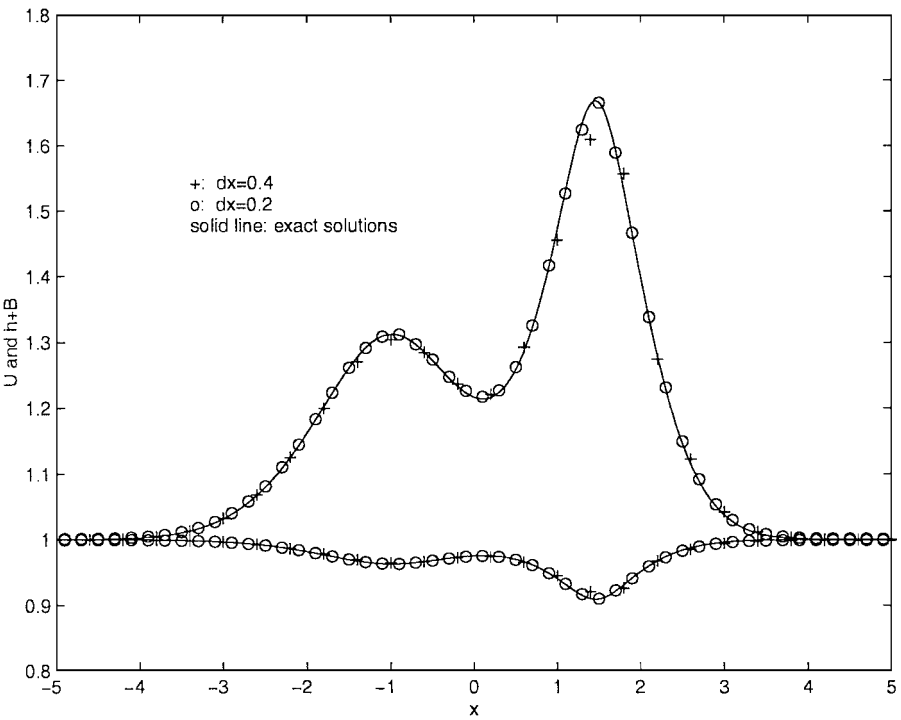


**FIG. 12.** The numerical solutions ($U$ and $h + B$) of Case 2, where 100 ($\bigcirc$) and 50 ($+$) grid points are used in the computational domain $x \in [-10, 10]$. The solid lines are exact solutions. The plot domain is $x \in [-5, 5]$.

where $L = 14{,}000$ m is the channel length. The initial and boundary conditions are

$$h(x, 0) = 60.5 - B(x), \quad U(x, 0) = 0,$$

and

$$h(0, t) = 64.5 - 4.0 \sin\left[\pi\left(\frac{4t}{86{,}400} + \frac{1}{2}\right)\right], \quad U(L, t) = 0.0.$$

With the above conditions, there is an approximate solution based on the asymptotic analysis given in [3],

$$h(x, t) = 64.5 - B(x) - 4 \sin\left[\pi\left(\frac{4t}{86{,}400} + \frac{1}{2}\right)\right],$$

and

$$U(x, t) = \frac{(x - L)\pi}{5400h(x, t)} \cos\left[\pi\left(\frac{4t}{86{,}400} + \frac{1}{2}\right)\right].$$

The simulations result from the BGK scheme at output time $t = 7552.13$ s with $\Delta x = 280$ m (50 cells in $L$) are presented in Figs. 13 and 14, where the solid lines are exact solutions. The agreement between the numerical and exact solutions are excellent.

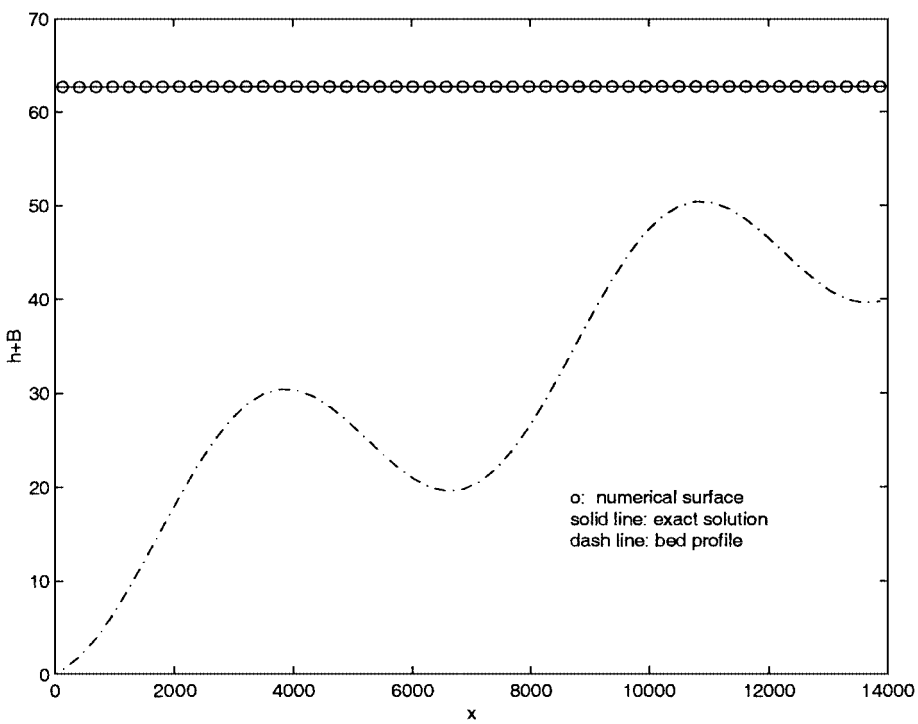


**FIG. 13.** Water-surface and river bottom distributions for Case 3. The circles are numerical solution calculated with 50 grid points and the solid line is the exact solution.

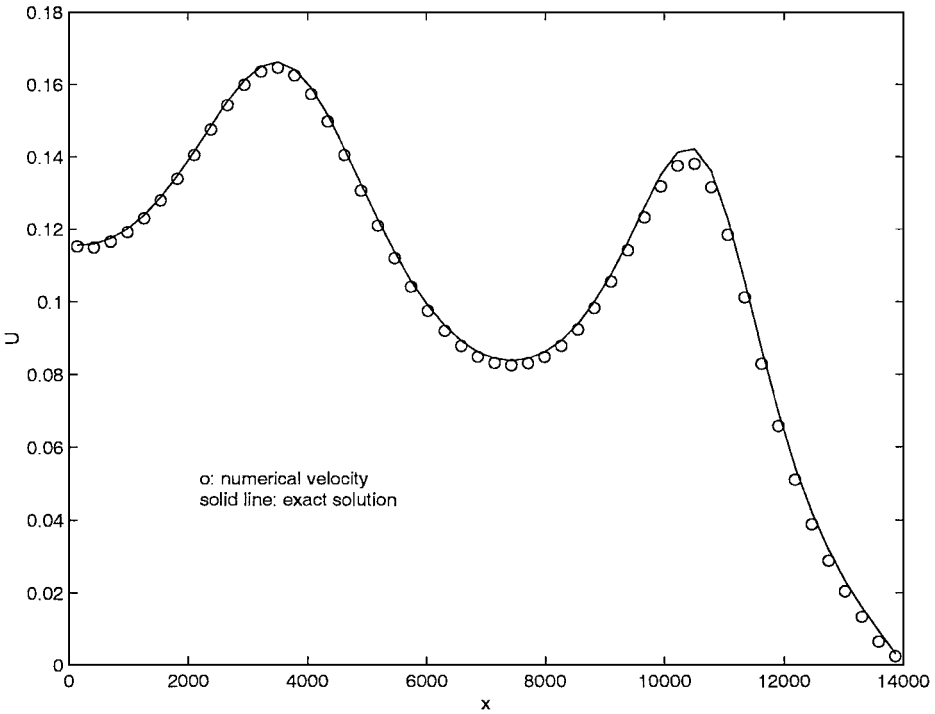


**FIG. 14.** Velocity distribution at time $t = 7552.13$ s. Fifty grid points are used in the calculation and the solid line is the analytic solution.

*Case 4*. These are classical test problems for transcritical and subcritical flows. They are widely used to test numerical schemes for the shallow-water equations. The 1D simulation channel has a length of 25 m. The bed profile is given by

$$B(x) = \begin{cases} 0.2 - 0.05(x - 10)^2 & \text{for } 8 < x < 12, \\ 0.0 & \text{otherwise.} \end{cases}$$

Depending on the initial and boundary conditions, the flow can be subcritical, transcritical with or without a steady shock, or supercritical. Since the transcritical cases are more difficult, we only include these two cases here. In both cases, the physical domain is covered with 200 cells with the cell size $\Delta x = 0.125$ m.

For the transcritical case without a shock, a discharge per unit width of $hU = 1.53$ m$^2$/s was imposed as the upstream boundary condition. The steady state solutions for both $hU$ and $h + B$ are shown in Figs. 15 and 16. As noticed by many authors, the correct capturing of the discharge $hU$ is usually more difficult than the water height $h + B$. For the transcritical flow with a shock, the discharge has a value $hU = 0.18$ m$^2$/s at the upstream boundary and $h = 0.33$ m is imposed as the downstream boundary condition. The simulation results of $hU$, $h + B$ and Froude number $Fr = U/\sqrt{Gh}$ are shown in Figs. 17–19. Like the scheme in [22], there exists an overshoot in the Fr distribution. In comparison with the results obtained from the KFVS-type kinetic method [2], the current method has a good accuracy, such as in the solution of flow discharge.

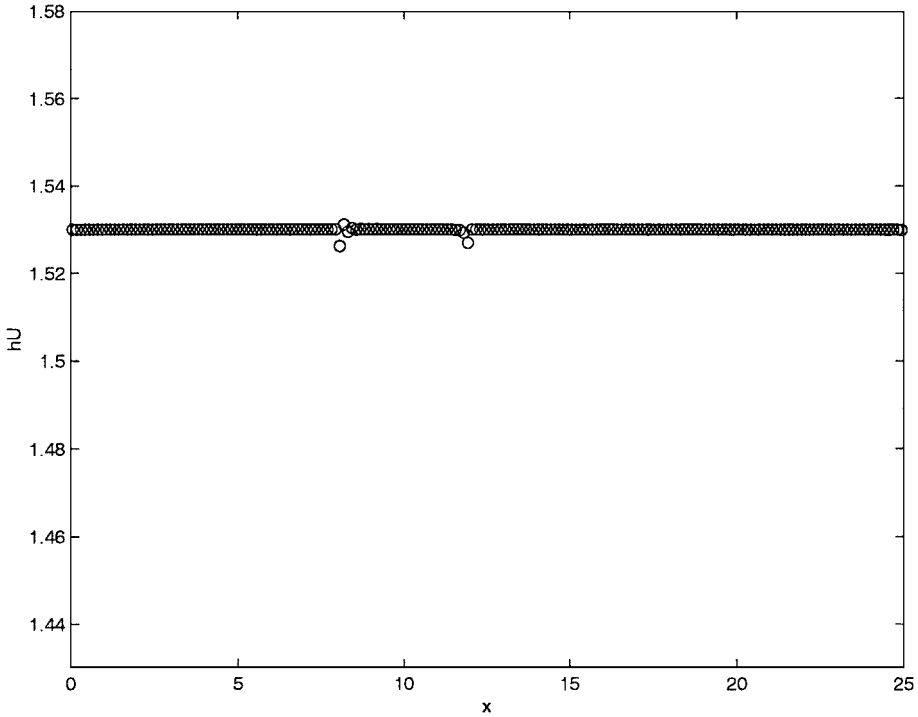


**FIG. 15.** Transcritical flow without a shock. Flow discharge $hU$ is plotted and the exact solution is $hU = 1.53$ m$^2$/s. In this case 200 grid points are used.

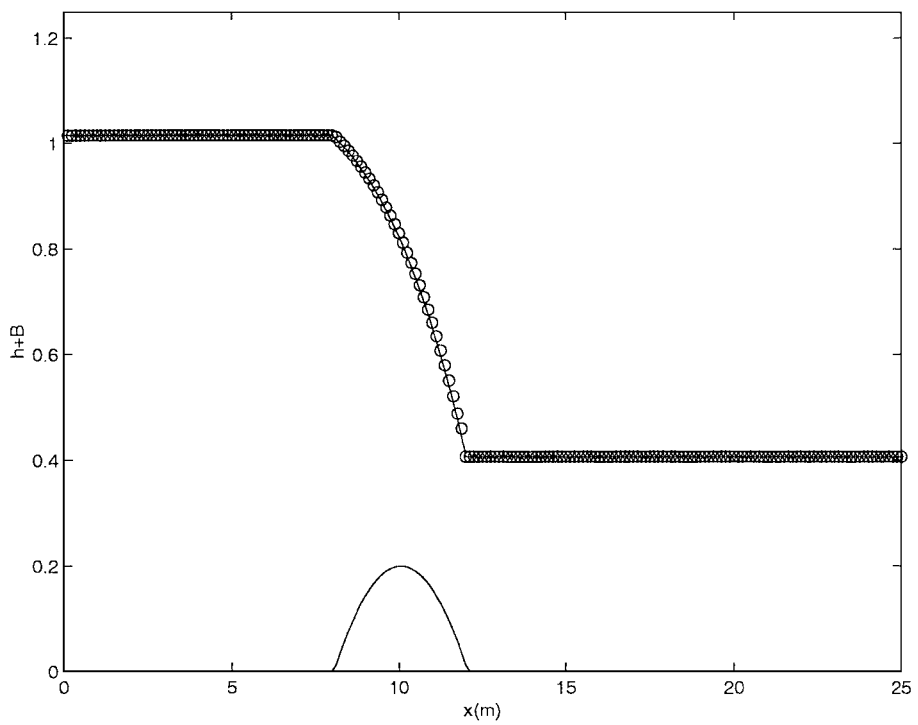


**FIG. 16.** Continuation of Fig. 15. Water surface height $h + B$.

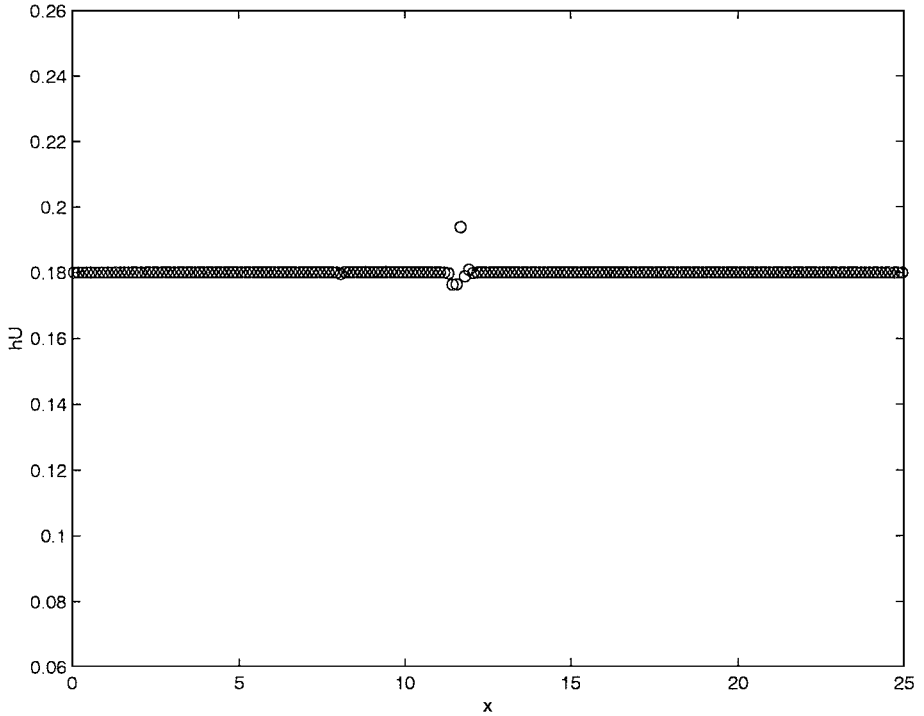


**FIG. 17.** Flow discharge $hU$ in transcritical flow with a shock case. The exact solution is $hU = 0.18$. Two hundred grid points are used in the calculation.

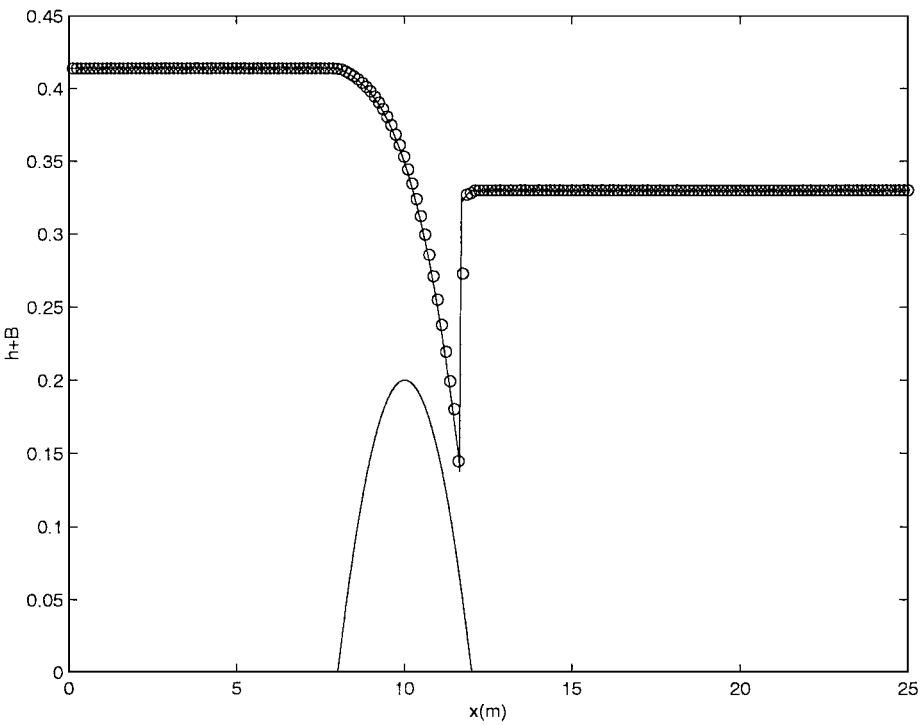


**FIG. 18.** Continuation of Fig. 17. Water surface distribution $h + B$.

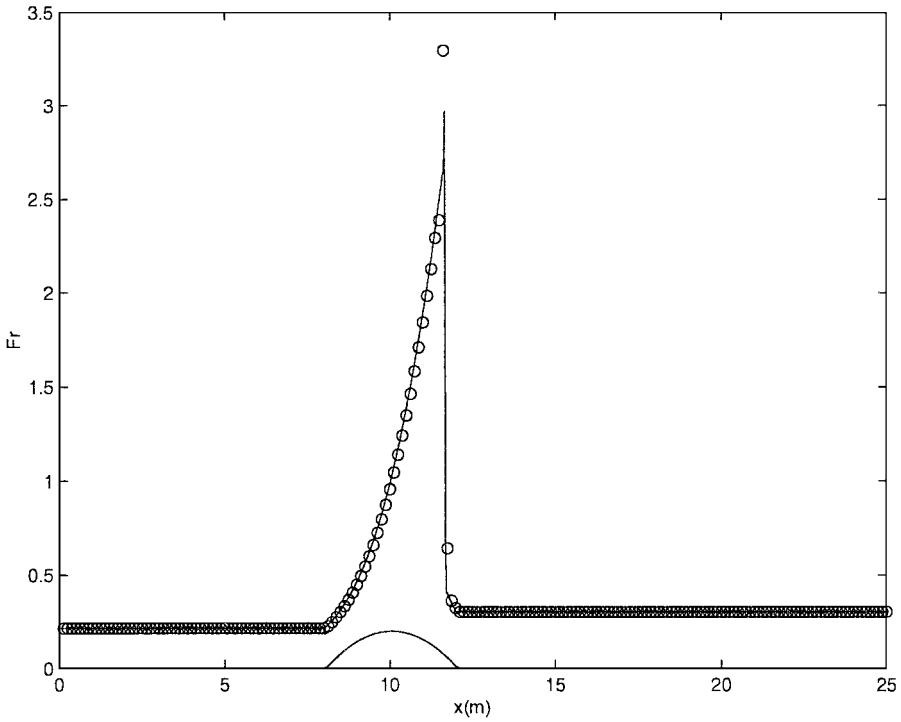


**FIG. 19.** Continuation of Fig. 17. Froude number $U/\sqrt{Gh}$ distribution.

*Case 5*. This case is about sound wave propagation, proposed by LeVeque in [14]. The channel has a length 1.0 and the channel bottom has the topography defined by

$$B(x) = \begin{cases} 0.25(\cos(\pi(x - 0.5)/0.1) + 1.0) & \text{for } |x - 0.5| \le 0.1, \\ 0.0 & \text{otherwise.} \end{cases}$$

The data are initially stationary ($U = 0$), with a surface profile defined by

$$h(x) = \begin{cases} 1.0 - B(x) + \epsilon & \text{for } 0.1 < x < 0.2, \\ 1.0 - B(x) & \text{otherwise.} \end{cases}$$

Two cases have been run with $\epsilon = 0.2$ and 0.01. The solutions with 100 and 200 grid points and $G = 1.0$ are shown in Figs. 20–23. The case with $\epsilon = 0.01$ is a very tough one. In order to get a smooth solution around the varying river bottom, an operator-splitting scheme (without source term effect in the flux function) needs definitely many more grid points than the well-balanced one to get the same resolution. Even for the well-balanced schemes, the use of 100 or 50 grid points may make their results differ, because many well-balanced schemes are designed so delicately on the stationary equilibrium solution. But the flow in this test case is in the quasisteady state. From this case, we can understand that the gas-kinetic scheme can capture the quasisteady solutions as well as LeVeque's scheme. But the kinetic scheme has no difficulty in capturing transcritical flow with shocks.

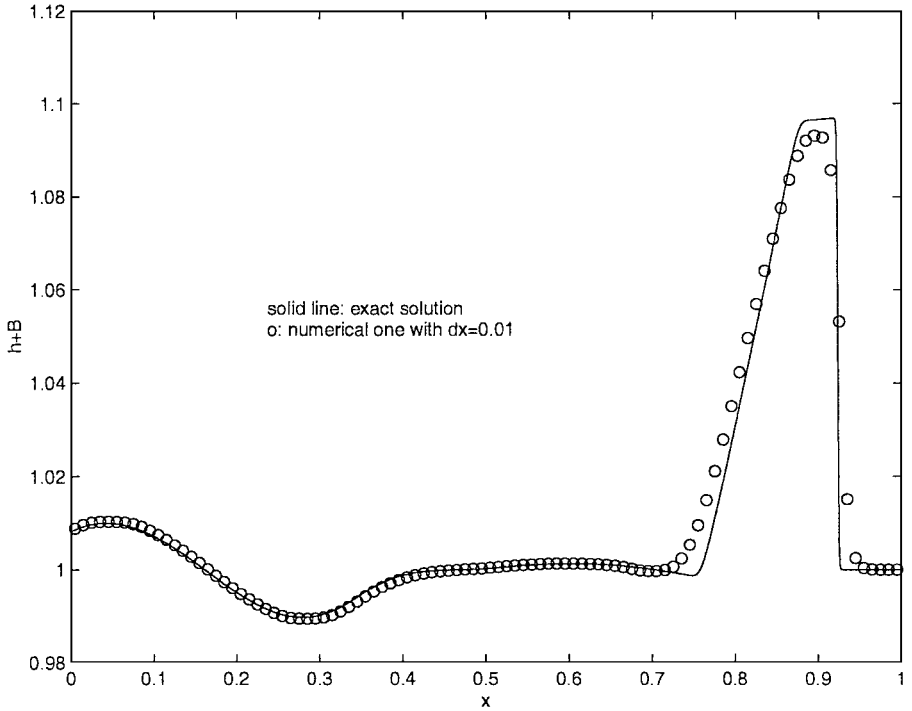


**FIG. 20.** Water height $h + B$ distribution in LeVeque's case with $\epsilon = 0.2$ and the output time $t = 0.7$. One hundred grid points are used in the calculation. The solid line is the numerical solution obtained with 1000 grid points.

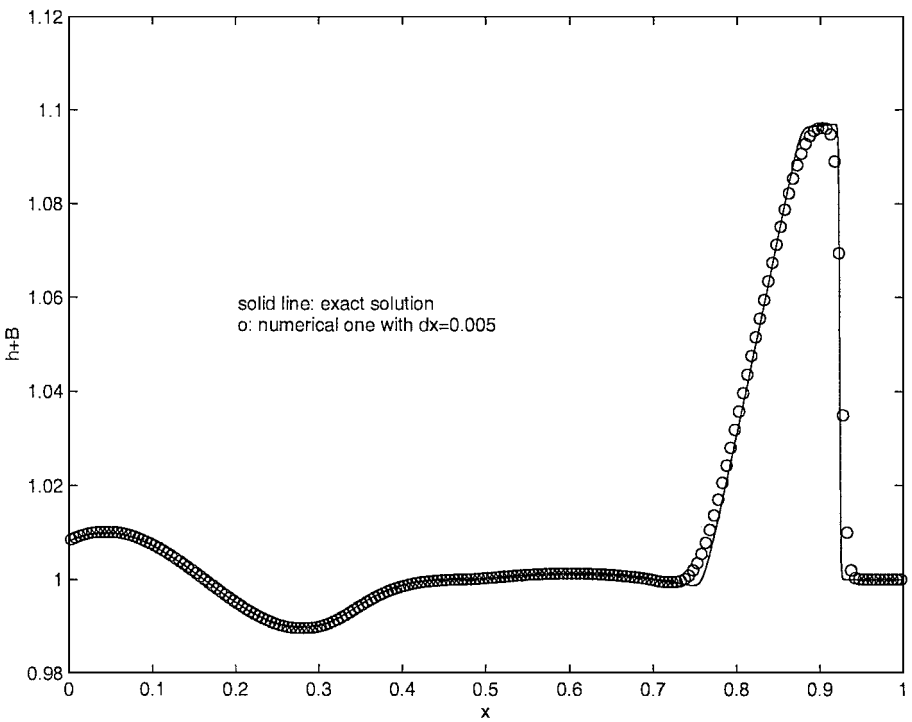


**FIG. 21.** Continuation of Fig. 20. Two hundred grid points are used.

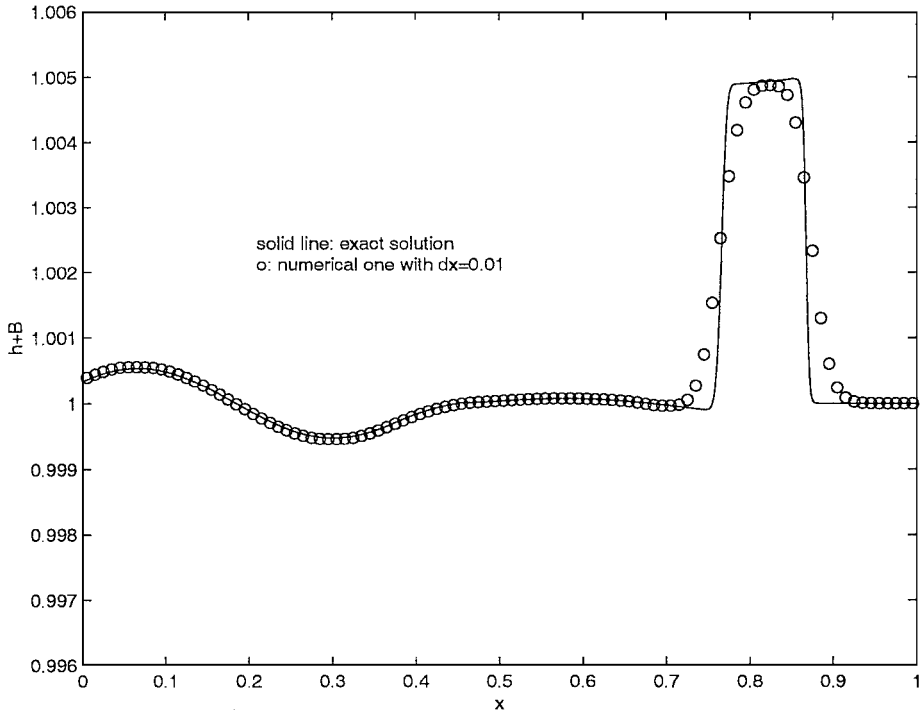


**FIG. 22.** Water height $h + B$ distribution in LeVeque's case with $\epsilon = 0.01$. The output time is $t = 0.7$. One hundred grid points are used. The solid line is the numerical solution obtained with 1000 grid points. Notice that the van Leer limiter is used for the initial data reconstruction.

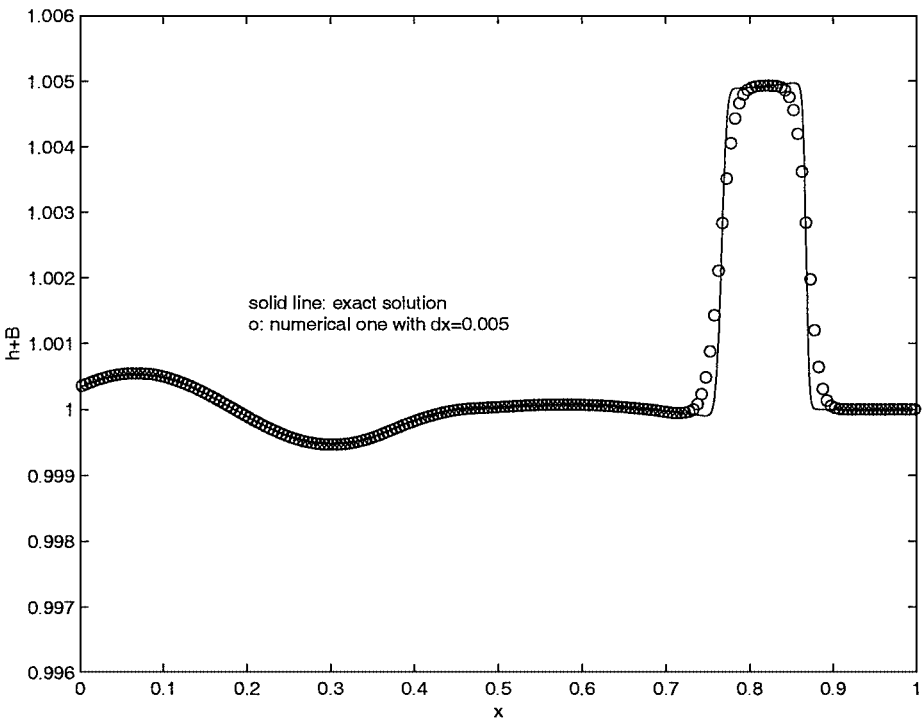


**FIG. 23.** Continuation of Fig. 22. Two hundred grid points are used.

**TABLE I**

**Max Norm of Deviation from Flatness in Water Surface ($h + B - 1$) at Times $t = 0.1$ and 1.0 for 2D Shallow-Water Equations in the Stationary Case on $N \times N$ Grids by the Current BGK Scheme and LeVeque's Method [14]**

| N | $t = 0.1$ (BGK) | $t = 1.0$ (BGK) | $t = 0.1$ (LeVeque) |
|---|---|---|---|
| 50 | $4.44 \times 10^{-16}$ | $1.33 \times 10^{-15}$ | $1.0 \times 10^{-3}$ |
| 100 | $6.66 \times 10^{-16}$ | $1.22 \times 10^{-15}$ | $2.5 \times 10^{-4}$ |
| 200 | $1.33 \times 10^{-15}$ | $9.99 \times 10^{-15}$ | $6.3 \times 10^{-5}$ |

The extension of the current BGK scheme to the 2D case using direction by the direction-splitting method is straightforward [21]. The gas distribution function at a cell interface will be the same as that in Eq. (2.21) except for additional $v$-velocity (in a perpendicular direction) dependence terms in all equilibrium states ($g_0$, $g^l$, $g^r$) and its Taylor expansion. In an earlier work, an operator-splitting BGK scheme [6], no gravitational term included in the flux function, was successfully implemented in many 2D engineering problems. In the following tests, we are going to test the current well-balanced BGK scheme on stationary and quasisteady flow simulations. In the following, we include three cases in two dimensions from LeVeque's paper [14], where $G = 1.0$ is used.

*Case 6.* This is a test about the capturing of the equilibrium state in a 2D case. The computational domain is $[0, 1] \times [0, 1]$ with a two-dimensional hump in the middle,

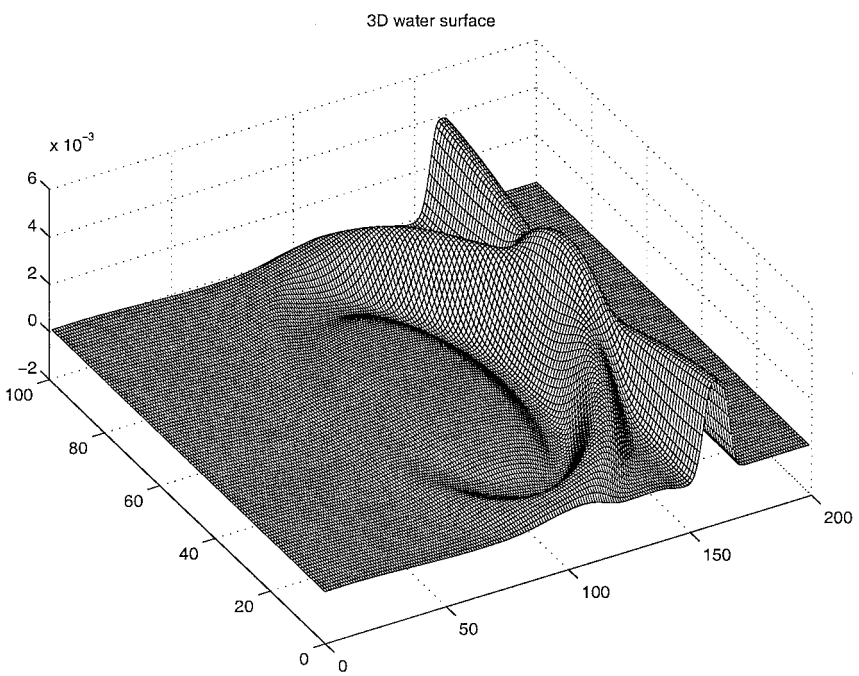


**FIG. 24.** Three-dimensional water surface for the test Case 6 with a circular-shaped bottom bump centered at (0.9, 0.5). The computational domain $[0, 2] \times [0, 1]$ is covered by $200 \times 100$ grid points. The initial water surface perturbation is at $0.05 < x < 0.15$ with magnitude $\epsilon = 0.01$.

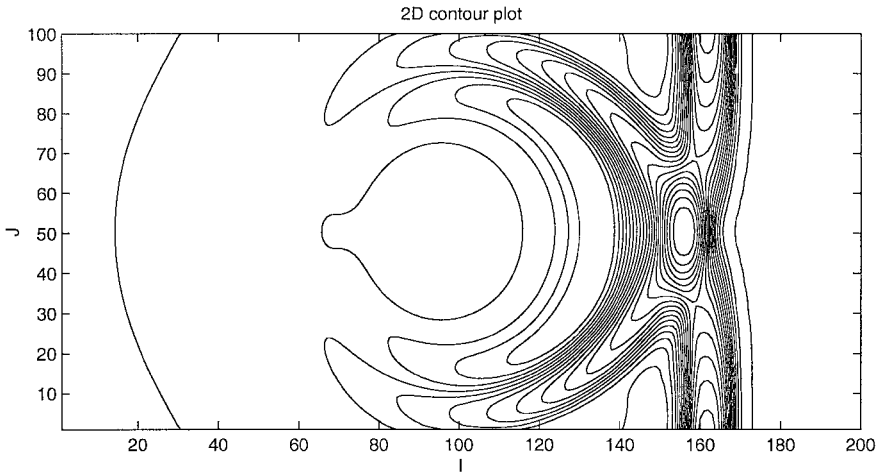


**FIG. 25.** Contours of the water surface shown in Fig. 24.

$$B(x, y) = 0.8 \exp(-50((x - 0.5)^2 + (y - 0.5)^2)).$$

The initial water depth is set to $h(x, y) = 1 - B(x, y)$ with zero velocity. So theoretically the surface should remain undisturbed. Table I shows the max norm of $(h + B) - 1$ at times $t = 0.1$ and 1.0 for the 2D BGK method on three different grids. Similarly to the 1D case, the BGK scheme could preserve the equilibrium solution to the machine limits.

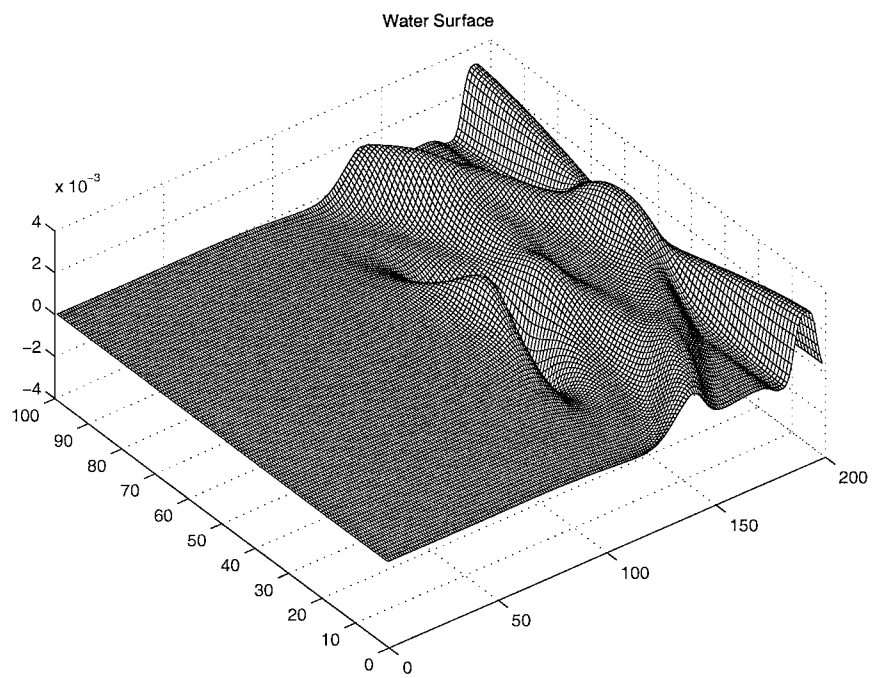


**FIG. 26.** Three-dimensional water surface for the test Case 7 with an elliptical bottom bump centered at (0.9, 0.5). The computational domain $[0, 2] \times [0, 1]$ is covered by $200 \times 100$ grid points. The initial water surface perturbation is at $0.05 < x < 0.15$ with magnitude $\epsilon = 0.01$.

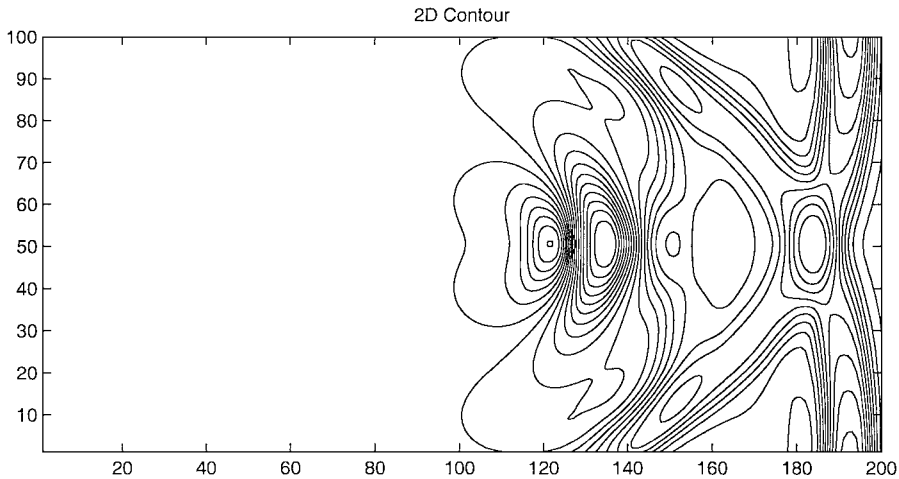


**FIG. 27.** Contours of water surface shown in Fig. 26.

With the shifted hump in the $x$ direction,

$$B(x, y) = 0.8 \exp(-50((x - 0.9)^2 + (y - 0.5)^2)),$$

and with an enlarged computational domain $[0, 2] \times [0, 1]$, we perturb the initial $h$ by $\epsilon = 0.01$ in the region $0.05 < x < 0.15$. Based on $200 \times 100$ grid points, the water surface distribution and its 2D contours are shown in Figs. 24 and 25, where smooth and symmetric water-surface distributions are presented.

*Case 7.* This is a case with the same flow perturbation as in Case 6 but with an isolated elliptical-shaped hump [14],

$$B(x, y) = 0.8 \exp(-5(x - 0.9)^2 - 50(y - 0.5)^2).$$

The computational domain is $[0, 2] \times [0, 1]$, which is covered by $200 \times 100$ grid points. The water surface and its contours at time $t = 1.8$ are shown in Figs. 26 and 27. Again, both figures show the smoothness of water-surface distributions.

## 4. CONCLUSION

In this paper, we have developed a gas-kinetic BGK scheme for the shallow-water equations with source term. The particle acceleration due to the gravitational force is explicitly included in fluid evolution and the construction of numerical fluxes. The current method is a well-balanced scheme and is a very robust method for both steady and unsteady flow simulations. Excellent simulation results are obtained for many tough problems. The success of the kinetic method comes from its underlying design principle: the numerical fluid evolution should follow the fluid physics as closely as possible. The physical reality for the shallow-water equations with the source term is that the gravitational force exists everywhere; it will effect not only the fluid movement inside each numerical cell (second term on the right hand side of Eq. (1.2)) but also the fluid particles passing through the cell interface

(first term on the right hand side of Eq. (1.2)). The importance of including a source term in the flux evaluation has been emphasized earlier for the Euler equations with heat transfer [20]. Even for the compressible Euler and Navier–Stokes equations, the success of the gas-kinetic BGK scheme in comparison with other flux vector splitting schemes (based on the collisionless Boltzmann equation) is also due to the including of source term (particle collisions) in the flux evaluation.

## ACKNOWLEDGMENTS

The author thanks the reviewers for their helpful comments which subsequently improved the current manuscript, such as the inclusion of the 2D cases. The current research is supported by the Research Grant Council of Hong Kong through HKUST6132/00P and DAG01/02.SC19.

## REFERENCES

1. F. Alcrudo and F. Benkhaldoun, Exact solutions to the Riemann problem of the shallow water equations with a bottom step, *Comput. Fluids* **30**, 643 (2001).
2. E. Audusse, M. O. Bristeau, and B. Perthame, *Kinetic Schemes for Saint-Venant Equations with Source Terms on Unstructured Grids*, INRIA Report No. 3989 (2000).
3. A. Bermudez and M. E. Vazquez, Upwind methods for hyperbolic conservation laws with source terms, *Comput. Fluids* **23**(8), 1049 (1994).
4. P. L. Bhatnagar, E. P. Gross, and M. Krook, A model for collision processes in gases. I: Small amplitude processes in charged and neutral one-component systems, *Phys. Rev.* **94**, 511 (1954).
5. V. T. Chow, *Open-Channel Hydraulics* (McGraw-Hill, New York, 1959).
6. M. S. Ghidaoui, J. Q. Deng, W. G. Gray, and K. Xu, A Boltzmann based model for open channel flows, *Int. J. Numer. Methods Fluids* **35**, 449 (2001).
7. P. Glaister, Approximate Riemann solutions of the shallow water equations, *J. Hydraul. Res.* **26**(3), 293 (1988).
8. J. M. Greenberg and A. Y. Lerroux, A well-balanced schemes for the numerical processing of source terms in hyperbolic equations, *SIAM J. Numer. Anal.* **33**(1), 1 (1996).
9. W. H. Hui and C. H. Pan, The water surface formulation for two-dimensional shallow water flow with bottom topography, preprint (2001).
10. M. E. Hubbard and P. Garcia-Navarro, Flux difference splitting and the balancing of source terms and flux gradients, *J. Comput. Phys.* **165**, 89 (2000).
11. P. Jenny and B. Muller, Rankine–Hugoniot–Riemann solver considering source terms and multidimensional effects, *J. Comput. Phys.* **145**, 575 (1998).
12. S. Jin, A steady-state capturing method for hyperbolic systems with geometrical source terms, *Math. Model Numer. Anal.* **35**, 631 (2001).
13. S. Jin and Y. J. Kim, On the computation of roll waves, *Math. Model Numer. Anal.* **35**, 463 (2001).
14. R. J. LeVeque, Balancing source terms and flux gradients in high-resolution Godunov methods: the quasisteady wave-propagation algorithm. *J. Comput. Phys.* **146**, 346 (1998).
15. A. Noussair, Riemann problem with nonlinear resonance effects and well-balanced Godunov scheme for shallow water fluid flow past an obstacle, *SIAM J. Numer. Anal.* **39**(1), 52 (2001).
16. B. Perthame and C. Simeoni, A kinetic scheme for the Saint-Venant system with a source term, *CALCOLO*, in press.
17. A. Slyz and K. H. Prendergast, Time-independent gravitational fields in the BGK scheme for hydrodynamics, *Astron. Astrophys. Suppl. Ser.* **139**, 199 (1999).
18. E. F. Toro, *Shock-Capturing Methods for Free-Surface Shallow Flows* (Wiley, New York, 2001).

19. M. E. Vazquez-Cendon, Improved treatment of source terms in upwind schemes for the shallow water equations in channels with irregular geometry, *J. Comput. Phys.* **148**, 497 (1999).
20. K. Xu, A gas-kinetic scheme for the Euler equations with heat transfer, *SIAM J. Sci. Comput.* **20**, 1317 (1999).
21. K. Xu, A gas-kinetic BGK scheme for the Navier–Stokes equations and its connection with artificial dissipation and Godunov method, *J. Comput. Phys.* **171**, 289 (2001).
22. J. G. Zhou, D. M. Causon, C. G. Mingham, and D. M. Ingram, The surface gradient method for the treatment of source terms in the shallow water equations, *J. Comput. Phys.* **168**, 1 (2001).